

V2HDM-Mono: A Framework of Building a Marking-Level HD Map with One or More Monocular Cameras

Hongji Liu, Linwei Zheng, Xiaoyang Yan, Zhenhua Xu, Bohuan Xue, Yang Yu and Ming Liu

Abstract—Marking-level high-definition maps (HD maps) are of great significance for autonomous vehicles, especially in large-scale, appearance-changing scenarios where autonomous vehicles rely on markings for localization and lanes for safe driving. In this paper, we propose a highly feasible framework for automatically building a marking-level HD map using a simple sensor setup (one or more monocular cameras). We optimize the position of the marking corners to fit the result of marking segmentation and simultaneously optimize the inverse perspective mapping (IPM) matrix of the corresponding camera to obtain an accurate transformation from the front view image to the bird’s-eye view (BEV). In the quantitative evaluation, the built HD map almost attains centimeter-level accuracy. The accuracy of the optimized IPM matrix is similar to that of the manual calibration. The method can also be generalized to build HD maps in a broader sense by increasing the types of recognizable markings. The supplementary materials and videos are available at <http://liuhongji.site/V2HDM-Mono/>.

I. INTRODUCTION

A. Motivation

HD maps are of great assistance to many modules of Unmanned Ground Vehicles (UGVs), such as localization, perception, and planning [1], especially in large-scale appearance-changing application scenarios where autonomous vehicles rely on markings for localization and lanes for safe driving [2]. With such demands, the coordinates of markings need to be accurate enough to assist the localization of UGVs. The IPM matrix converting camera images to BEV also needs to be precise enough in order to ensure the calculation accuracy of the distance between the vehicle and lanes. Moreover, there are usually a great number of markings in large-scale scenes. In practical application, the generation of such HD maps is highly dependent on manual measurement with surveying and mapping tools such as Total Station [2], the workload is huge, and the measurement process takes a very long time. Therefore, it is of interest to the community to build the HD marking map automatically.

With the development of intelligent driving technologies, IPM has been successfully applied to many intelligent driving problems, mainly for obtaining the BEV around the vehicle. It can facilitate road and obstacle detection [3], free

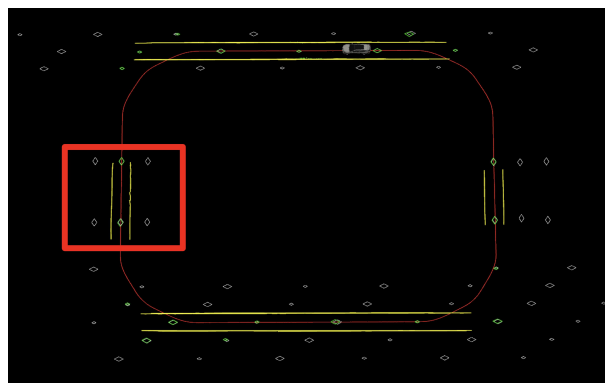
Hongji Liu, Linwei Zheng, Xiaoyang Yan, Zhenhua Xu, Bohuan Xue are with The Hong Kong University of Science and Technology, Hong Kong SAR, China. (e-mail: hliucq@connect.ust.hk)

Yang Yu and Ming Liu are with The Hong Kong University of Science and Technology (Guangzhou), Nansha, Guangzhou, 511400, Guangdong, China,

Ming Liu is also with The Hong Kong University of Science and Technology, Hong Kong SAR, China, and with HKUST Shenzhen-Hong Kong Collaborative Innovation Research Institute, Futian, Shenzhen. (e-mail: eelium@ust.hk)



(a) Aerial view of the experimental scene



(b) Automatically generated partial marking HD map

Fig. 1. An example of building an HD map in an automated port. Fig. 1(a) is an aerial photograph of the whole scene. Fig. 1(b) is an example of an HD map established within the coverage of the experimental trajectory. The yellow line segments are the lanes in the actual scene. The green markings are automatically generated by the proposed method. The white markings are the real markings in the scene. The positions circled in red boxes in Fig. 1(a) and Fig. 1(b) are corresponding. Please zoom in for details.

space estimation [4], lane keeping [2], autonomous parking, local planning and even optical flow computation [5]. However, the calibration of the IPM matrix with Total Station is time-consuming and laborious, which brings additional costs. Therefore, proposing a more convenient calibration method without human participation will be of great value.

Given the motives mentioned above, we propose combining the task of obtaining an accurate IPM matrix with building HD maps and solving them simultaneously. LiDAR-based methods are limited due to the deployed expensive sensors and time-consuming computation. Cameras are inexpensive and easy to deploy sensors, which are very friendly for low-cost UGV applications, and almost all UGVs can be equipped with cameras. In order to make our method applicable to as many kinds of UGVs as possible, we seek

to accomplish this task through a simple sensor setup: one or more monocular cameras.

Completing this task with only monocular camera(s) is quite challenging. There will be some problems if we just inverse project the target points in the image to the ground plane (naive IPM method) to build the HD map. First, the IPM matrix possesses a significant error without calibration. Secondly, the camera's position will change slightly with the movement of the UGV, which will also bring a huge random error to the inverse projection. Hence the precision of the map constructed by naive IPM is unsatisfactory. In scenes with many close identical markings, it is confusing to determine the corresponding relationship between the markings observed and the markings in the map. The IPM matrix has 8 degrees of freedom, which requires many constraints and is very complex to calculate.

We first convert the road marking corners and lane points segmented in the image into the map frame using IPM and the corresponding vehicle pose. Then we optimize the position of road markings and IPM matrix together to make the road markings projected on the image plane as consistent with the observation as possible.

The method can be generalized to build any road marking-level HD maps in a broader sense by changing the types of recognizable markings to the specific markings in target scenarios. For example, if an HD map is applied to open roads in urban scenes, the markings should be various common traffic markings on the road.

B. Contribution

We summarize our contribution as follows:

- 1) We proposed a simple yet feasible framework for building a marking-level HD map using one or more monocular cameras.
- 2) In the above framework, in addition to building an HD map, the IPM matrix of the used camera can also be optimized simultaneously.
- 3) We collected experimental data in two different practical application scenarios and verified the feasibility and accuracy of the method using two indexes of RMSE and IoU, respectively. The RMSE of the marking corners in the final marking map can be close to the centimeter level. The average IoU of generated markings with ground truth can achieve 60%-70%. The optimized IPM matrix can achieve the same accuracy as manual calibration.

II. RELATED WORK

A. BEV-based Estimation

In recent years, there has been much research on converting image(s) perpendicular to the ground to the BEV, which is used for downstream tasks, such as local planning, road elements estimation, and HD map construction. Yang *et al.* [6] proposed to leverage a cycle structure and a cross-view transformer that correlates views attentively to facilitate the road scene layout estimation. Guo *et al.* [7] proposed a low-cost method using normal sensor setup in contemporary cars

to generate BEV images and then a lane graph of the road. The methods proposed in [8]–[12] could use only monocular camera images to generate semantic maps in the BEV.

However, the normal sensor setup limited the field of view of BEV images, so some methods used multiple images around the vehicle to reconstruct a complete surrounding map in BEV. Pan *et al.* [4] proposed VPN to parse the first-view observations from multiple angles into a BEV semantic map. Phillion *et al.* [13] inferred road semantics directly in the BEV inferred from arbitrary camera rigs. Li *et al.* [14] proposed HDMaPNet. It can work with either or both images and point clouds. Based on semantic segmentation, vectorized maps can also be generated. Deng *et al.* [15] proposed a method specifically designed to generate the BEV using multiple panoramic cameras. However, UGVs used in real scenes always are not equipped with several cameras to provide sufficient multiple-view image data.

The results of all the above methods are limited to semantic segmentation rather than an HD map with accurate target coordinates.

B. HD Map Construction

In order to get the precise location of the target marking, researchers have also made many contributions to building HD maps. HD maps include many elements, such as curbs, the lane network, road markings, semantic traffic objects, lane center lines, and so on. Recently, different methods targeting different components of the HD map are beginning to flourish. Can *et al.* [16] predict the lane topology from only one on-board image. Xu *et al.* [17] [18] [19] [20] contributed a lot in road curb and boundary extraction from aerial images. Most related work focuses on establishing road, lane, and road markings maps.

Shu *et al.* [21] used raw crowdsourcing GPS trajectories data to build a lane-level map with both efficiency and accuracy improvement. Mi *et al.* [22] proposed a hierarchical graph generative model to generate the HD lane map in a data-driven way.

Some researchers have tried to obtain the exact location of the markings. Cheng *et al.* [23] extracted the sparse key points of the road markings and used Visual-Inertial Odometry (VIO) to optimize the map and the vehicle poses at the same time. Some methods used the 3D information from LiDAR to inverse project camera data into the point cloud to obtain HD maps. Elhousni *et al.* [24] inverse projected the road surface, curb, and lane segmentation results in the images onto the point cloud directly with the calibrated transformation between the camera and LiDAR. Zhou *et al.* [25] inverse projected the image segmentation results onto the ground plane extracted from point cloud data. Both of them need the help of the point cloud to acquire real-world coordinates. Whereas in some low-cost and simple UGV applications, LiDAR may not be equipped.

Some methods similar to our idea utilized IPM to inverse project the elements in the image into the world coordinate frame. Ranganathan *et al.* [26] used IPM to inverse project the front-view image to BEV, then detected FAST corners

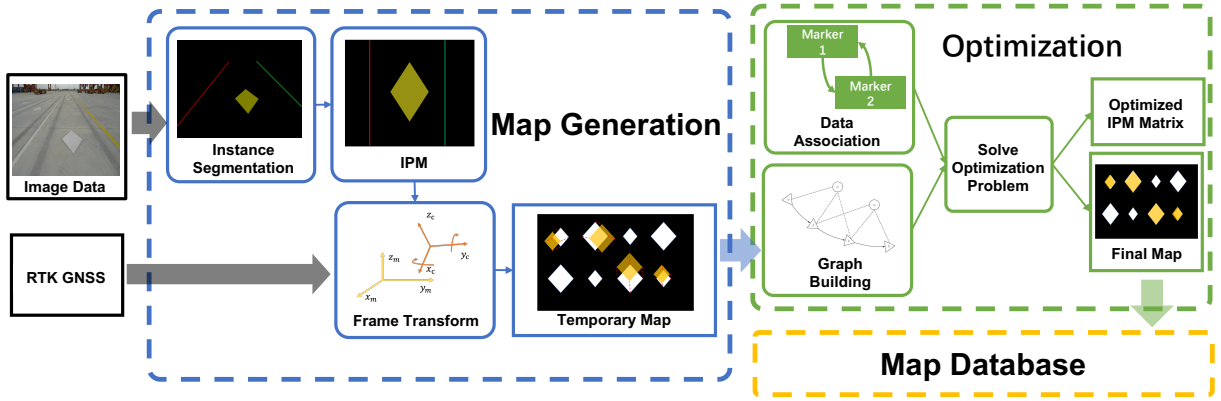


Fig. 2. The inputs of our system are any number of monocular camera images and the corresponding vehicle poses obtained from RTK-GNSS. The markings extraction module recognizes the markings and lanes in the image and extracts the key points. The map generation module uses IPM to inverse project the extracted key points into the vehicle frame and then transforms them into map coordinate frame according to the vehicle pose information. Whenever a new marking is added to the map, the optimization module will conduct data association and solve the optimization problem to get the optimized map and IPM matrix.



Fig. 3. IPM matrix calibration example image.

within the maximally stable extremal regions (MSER). Jang *et al.* [27] used the idea of graph optimization to abstract lane elements into nodes to build lane level HD map. Then in [28], they further abstracted the markings into nodes in the graph and optimized them together with the poses of the vehicle. Qin *et al.* [29] proposed a lightweight and highly feasible method for building HD maps. They used IPM and vehicle pose information to transform the elements segmented in the image into the map coordinate frame. Then they used graph optimization to help get better vehicle poses so that the elements' positions become more accurate accordingly. However, the IPM matrix on which these methods depend also possesses errors. Having better vehicle poses does not guarantee that a more accurate map can be established. In addition, none of the above methods mentioned the data association problem. In a scenario with many similar and close markings, it is challenging to judge whether the markings observed in the current frame and the markings observed in the previous frames are the same. Therefore, there is a potential risk of erroneous data association in the subsequent optimization process.

III. METHODOLOGY

A. Problem Statement & System Overview

We formulate the whole problem as a maximum likelihood estimation (MLE) [30] for all the measurements during the data collection run:

$$\hat{\mathcal{X}} = \operatorname{argmax}_{\mathcal{X}} p(\mathcal{Z}|\mathcal{X}) = \operatorname{argmin}_{\mathcal{X}} \sum_k f(\mathcal{X}_k, \mathbf{z}_k) \quad (1)$$

where \mathcal{Z} is the set of all measurements \mathbf{z}_k for the marking corners that are independent of each other. \mathcal{X} is the set of all the variables, including the IPM and the 3D coordinates of marking corners in the map frame. $f(\cdot)$ is the objective function. Assuming the measurement follows the Gaussian distribution, problem (2) can be solved as a nonlinear least-squares problem:

$$\hat{\mathcal{X}} = \operatorname{argmin}_{\mathcal{X}} \sum_k \|\mathbf{r}(\mathcal{X}_k, \mathbf{z}_k)\|_{\sigma}^2, \quad (2)$$

where σ is the covariance. Such a problem can be solved usually using iterative methods such as Gauss-Newton or Levenberg-Marquardt.

In general, the inputs of our system are any number of monocular camera images and the corresponding vehicle poses. In our experimental scenarios, the vehicle poses are obtained from RTK-GNSS. The markings extraction module recognizes the markings and lanes in the image and extracts the key points. The map generation module constructs a temporary map using a naive strategy which will be elaborated in section III-C.2. Every time a new marking is added to the map, the optimization module will optimize the location of the markings in the whole map and the IPM matrix. Refer to Fig. 2 for the framework of the whole system.

B. Road Marking Detection

In our system, we use Meta AI Research's detection and segmentation algorithms library Detectron2 [31] to detect the contour of the ground markings (diamonds in our experimental scenario). For the lane detection task, we use UFLD [32] for its remarkable speed and accuracy.

C. IPM

We assume that the ground is flat and all the markings are on the ground plane (z equals 0). The IPM process can be defined as the following transformation [33]:

$$\mathbf{p}_2 = \mathbf{H}\mathbf{p}_1, \quad (3)$$

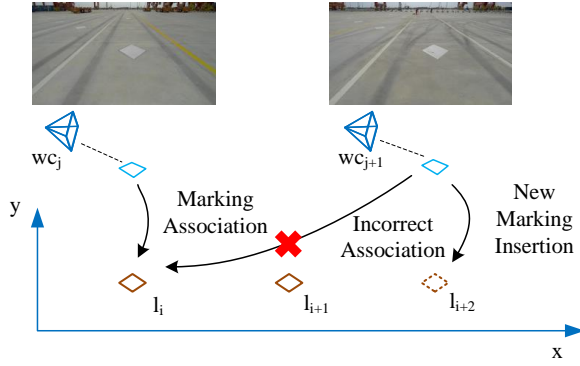


Fig. 4. An example of data association. The two images in the above figure are from different markings. If they are not discriminated against, there will be a problem that markings are incorrectly associated because the appearance of markings is the same.

expand the above formula to get:

$$s \begin{pmatrix} x \\ y \\ 1 \end{pmatrix} = \begin{pmatrix} h_1 & h_2 & h_3 \\ h_4 & h_5 & h_6 \\ h_7 & h_8 & 1 \end{pmatrix} \begin{pmatrix} u \\ v \\ 1 \end{pmatrix}, \quad (4)$$

where (x, y) is the coordinate of the point in the vehicle frame after the inverse projection transformation.

1) *Pre-calibration*: We use the multiple point pairs method to calculate the above-mentioned \mathbf{H} matrix. Firstly, we manually mark the target corners in the picture to obtain their pixel coordinates as in Fig. 3. On the experimental site, we invite professional surveying and mapping personnel to use Total Station to obtain the coordinates of the target corners in the vehicle frame. This way, we obtained 10 point pairs and can easily calculate the homography matrix.

2) *Naive Strategy*: After obtaining the marking detection result, a polygon is used to fit the contour of the segmentation results in the image. Then the polygon's corners are used as the keypoints to represent the marking. The simplest way to build the map is to directly inverse project the keypoints extracted from the image into the vehicle frame by equation (4), then transform them into the map frame according to the vehicle pose. We use the average coordinate as the final coordinate for those markings observed many times. Because the farther the target point is from the vehicle body, the greater the error of the IPM. Therefore, we take the region determined by the outermost calibration points, which is close to the camera center as the Region of Interest (ROI) used. Only pixels within the ROI will be inverse projected.

D. Optimization

To minimize the displacement of the inverse projected markings, instead of directly fitting the contours [28] after projecting them to the ground plane, we pursue to estimate an optimal homography matrix \mathbf{H} and the position of markings' corners at the same time to minimize the projection error.

1) *Data Association*: A good data association is required among the markings observed in different frames. Otherwise, there are possibilities that different markings are considered the same as depicted in Fig. 4. Our data association strategy consists of three major procedures. (1) The data preprocess-

ing for the segmentation results of detected markings. (2) The association of the individual markings. (3) The association of the corners within the markings.

In the first procedure, marking keypoints are extracted and transformed to map frame as described in III-C.2. In the second step, the geometric center of corners of a marking is calculated, and a quad-tree is maintained to store the center point. An incoming marking is associated with an existing marking if the center distance to the searched candidate is lower than a threshold. Otherwise, the new marking is inserted into the quad-tree as a new element. Finally, the corner correspondence of the marking is obtained by finding the minimal total corresponding corners' distance of all the candidate pairs.

2) *Minimization of Marking Detection Error*: The re-projection relation from the marking corner positions in the Euclidean space to the image pixel plane follows the equation:

$$\lambda \begin{bmatrix} u \\ v \\ 1 \end{bmatrix} = \mathbf{K}[\mathbf{R}_{cb}|\mathbf{t}_{cb}][\mathbf{R}_{wb}|\mathbf{t}_{wb}]^{-1} \begin{bmatrix} x_w \\ y_w \\ z_w \\ 1 \end{bmatrix}, \quad (5)$$

where \mathbf{K} is the intrinsic matrix. $[\mathbf{R}_{cb}|\mathbf{t}_{cb}]$ and $[\mathbf{R}_{wb}|\mathbf{t}_{wb}]$ are the transformation matrix of the camera extrinsic from camera frame to vehicle frame and vehicle pose, respectively. Therefore, the homography matrix \mathbf{H} which inverse project pixel coordinates from the image plane to the coordinates on the ground plane in the vehicle frame, can be written as a combination of the intrinsic and extrinsic of the camera as follows:

$$\begin{bmatrix} x_b \\ y_b \\ 1 \end{bmatrix} = \mathbf{H} \cdot \lambda \begin{bmatrix} u \\ v \\ 1 \end{bmatrix}, \quad (6)$$

$$\text{with } \begin{bmatrix} x_w \\ y_w \\ 1 \end{bmatrix} = [\mathbf{R}_{wb} \text{ col:1,2}|\mathbf{t}_{wb}] \begin{bmatrix} x_b \\ y_b \\ 1 \end{bmatrix},$$

$$\mathbf{H} = [\mathbf{R}_{cb} \text{ col:1,2}|\mathbf{t}_{cb}]^{-1} \mathbf{K}^{-1}.$$

The third column of the rotation matrix can be omitted, leveraging the fact that the inverse projected points are on the ground plane.

To build an HD map, we treat the problem as a bundle adjustment to estimate the homography matrix \mathbf{H} and the positions of the markings simultaneously. An illustration figure of the factor graph is shown in Fig. 5.

As the camera's intrinsic matrix \mathbf{K} is relatively easy to obtain, we assume it is well-calibrated and known. We also deem the vehicle poses $[\mathbf{R}_{wb}|\mathbf{t}_{wb}]$ acquired from RTK-GNSS accurate. The problem of optimizing \mathbf{H} matrix thus can be converted to optimizing the extrinsic matrix from the camera frame to the vehicle frame.

Since the vehicle lacks the rotation motion, which causes a degeneration of the translation part of the extrinsic matrix, a translation prior (installation position of the camera on the vehicle), according to the installation drawings provided by the UGV manufacturer, is used to constrain the extrinsic

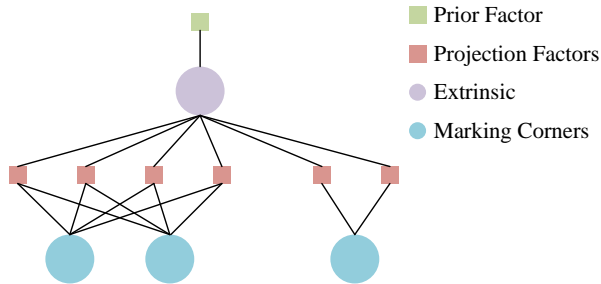


Fig. 5. The illustration of the factor graph of the bundle adjustment.

matrix. The initial guess of the extrinsic rotation matrix complies with the assumption that the xy -plane of the vehicle coordinate frame are parallel to the ground, the z -axis is vertical to the ground and upward, the z -axis of the camera coordinate frame is parallel to the ground and forward, and the y -axis is vertical to the ground and downward.

The initial guess of each marking corner's position is provided by the coarse IPM matrix using the naive strategy as in III-C.2 at the beginning and then provided by a transformation composed of extrinsic and intrinsic as equation (6) after the first iteration.

With variable \mathcal{X} containing the estimations for camera extrinsic and marking corners, equation (2) can be elaborated as the following equation:

$$\begin{aligned} \hat{\mathcal{X}} &= \{\hat{\mathbf{R}}_{cb}, \hat{\mathbf{t}}_{cb}, \hat{\mathbf{l}}_0 \dots \hat{\mathbf{l}}_n\} \\ &= \underset{\mathbf{R}_{cb}, \mathbf{t}_{cb}, \mathbf{l}_0 \dots \mathbf{l}_n}{\operatorname{argmin}} \left\{ \sum_{i \in [1, 4n], j \in [1, m]} f(i, j) \|\pi_{ij}(\mathbf{l}_i) - \mathbf{z}_{ij}\|_{\sigma}^2 \right. \\ &\quad \left. + \|\mathbf{t}_{cb} - \mathbf{t}_0\|_{\sigma}^2 \right\} \end{aligned} \quad (7)$$

where \mathbf{l}_i represents the 3D coordinate of the marking corner in the map frame. The total number of \mathbf{l}_i is $4n$ because there are 4 corners in each diamond marking. $f(i, j)$ equals to 1, if the marking corner \mathbf{l}_i can be observed from the j th pose, otherwise it equals to 0. π_{ij} follows (5) projecting the marking corner \mathbf{l}_i to the image pixel according to the j th pose. And \mathbf{z}_{ij} is the pixel measurement for \mathbf{l}_i observed from j th pose. The prior \mathbf{t}_0 is used to constrain the translation part of the camera extrinsic.

IV. EXPERIMENTAL RESULTS

A. Data Source

Our task is to build a marking level HD map. As far as we know, the existing public HD map data sets can not provide the marking coordinates ground truth. Therefore, we select two automated ports that rely on painting diamond markings on the ground to complete the visual localization of UGV to collect experimental data. The data includes markings CAD map of the field and vehicle-mounted sensors' data.

There are hundreds of markings totally in these two fields, respectively, and dozens of markings within the coverage of the experimental data collection route. There are lanes in both areas to ensure the safe operation of UGV.

B. Baselines

In order to verify the accuracy of HD map and IPM matrix generated by our method, we select the following baselines for comparative experiments.

- 1) **Calibrated Naive IPM (CNI):** The pre-calibrated IPM matrix is used to conduct the naive strategy, which was described in Section III-C.2
- 2) **Estimated Naive IPM (ENI):** It is the same as the above method, but the pre-calibrated IPM matrix comes from a different UGV. It means that the IPM matrix is inaccurate because the mechanical structures of different UGVs are quite different.
- 3) **Optimization (Opt):** Use the naive strategy to inverse project the corners of the markings into the vehicle frame, then optimize the corners' position and IPM matrix of the corresponding monocular camera.
- 4) **Optimized Naive IPM (ONI):** Conduct the naive strategy with the IPM matrix optimized by the optimization process.
- 5) **With One or More Monocular Cameras:** In our experiments, we use the front-mounted monocular camera, the rear-mounted monocular camera and both for comparison. When multiple cameras are used, each camera executes the above method separately.

C. Results

1) *Generated Maps:* The marking level HD map generated by our method in our second test scenario is shown in Fig. 1. The comparison of the partial HD map built with the inaccurate IPM matrix and the method proposed is shown in Fig. 7. There is a significant error between the markings generated by ENI and the ground truth. The markings generated by ONI coincide with the ground truth better.

2) *Quantitative Results:* In this section, we quantitatively compare the maps generated by different methods. Here we use two quantitative indexes, namely Root Mean Squared Error (RMSE) of marking corners and Intersection over Union (IoU) of marking.

- * **RMSE Index:** Calculate the RMSE of the corners of all markings with ground truth. This is used to measure the corner accuracy of the map.
- * **IoU Index:** We calculate the bounding box of an area jointly determined by the marking ground truth and the corresponding generated marking. The area is rasterized with grids of size $0.1M \times 0.1M$. Then we calculate the IoU of the number of grids occupied by the two markings.)

The RMSE index can show the accuracy of marking corners in the generated map. However, sometimes a relatively small RMSE can also be reached when the size and shape of the generated marking are quite different from the ground truth (because the corners of a marking are optimized separately). IoU index can avoid being affected by this situation.

In our first test scenario, we obtain the accurate IPM matrix for the front and rear monocular cameras using the

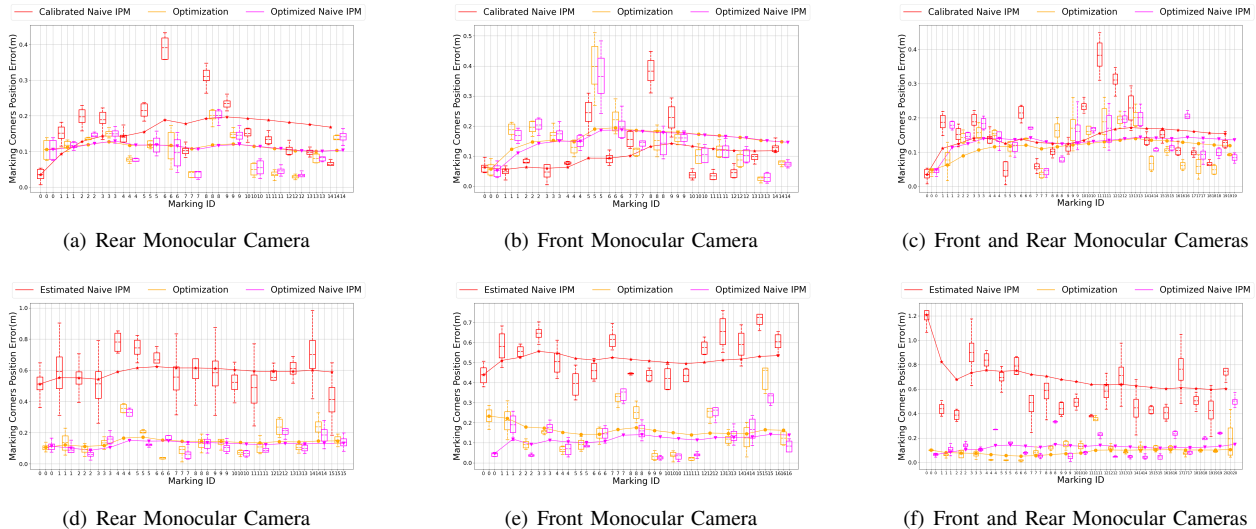


Fig. 6. Marking error comparison in two scenarios. The maps generated in the first scenario by CNI, Opt, and ONI with different monocular cameras are shown in 6(a) 6(b) 6(c). The maps generated in the second scenario by ENI, Opt, and ONI with different monocular cameras are shown in 6(d) 6(e) 6(f). The boxes represent the position error of the four corners in each marking, and the line with the corresponding color represents the change of the average corners position error of all markings with the increase of markings in the map. The position error is the Euclidean distance from the ground truth.

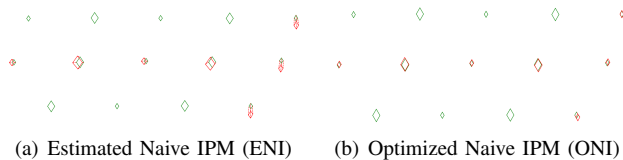


Fig. 7. The comparison between the maps generated by baselines and the ground truth. The green markings are the ground truth. The red markings are generated by baselines. The corner corresponding relationship is marked by red dash lines.

TABLE I

MAP ACCURACY STATISTICAL DATA EVALUATED USING RMSE AND IoU. THE BEST RESULTS IN A SCENARIO ARE MARKED IN BOLD. THE UNIT OF RMSE IS METER.

Scenarios/Baselines	Camera Setup						
	Front		Rear		Both		
	RMSE ↓	IoU ↑	RMSE ↓	IoU ↑	RMSE ↓	IoU ↑	
Scenario I	CNI	0.15	0.74	0.19	0.67	0.18	0.67
	Opt	0.17	0.71	0.12	0.77	0.13	0.74
	ONI	0.17	0.71	0.12	0.77	0.15	0.71
Scenario II	ENI	0.55	0.17	0.61	0.21	0.65	0.18
	Opt	0.21	0.63	0.17	0.65	0.13	0.72
	ONI	0.18	0.67	0.15	0.65	0.19	0.61

pre-calibration method described in Section. III-C.1. The error comparison of generated map from different baselines is shown in Fig. 6(a) 6(b) 6(c).

Due to the existence of calibration error, the accuracy of the IPM matrix calibrated for different cameras is different. Under different camera setups, our optimization method can reach similar accuracy to the CNI baseline, and the RMSE of the marking corners in the map is close to the centimeter level. Using the ONI method can achieve similar accuracy to the CNI shows that our method can obtain an IPM matrix with similar accuracy to the manual calibration while building the map. Thus, our method can replace the tedious

process of manually calibrating the IPM matrix.

We used a different UGV to collect experiment data in our second test scenario but still use the same IPM matrix. Due to the different mechanical structures of different vehicles, this IPM matrix is inaccurate. Under such conditions, the error comparison between generated maps from different methods is shown in Fig. 6(d) 6(e) 6(f).

It can be seen from the results that the accuracy of ENI is much lower because of the inaccurate IPM matrix. However, our optimization method can still build a map with an accuracy close to the centimeter level under such conditions. Using ONI mapping can still achieve the same accuracy as CNI mapping shows that even if we do not provide an accurate IPM matrix beforehand, the accuracy of the result map and optimized IPM matrix is not affected. This further reduces the difficulty of large-scale deployment of our method. It is not necessary to calibrate the IPM matrix for each vehicle. Instead, we can use a coarse one as a prior and optimize it during the mapping process.

To clarify the map error evaluation results, we list the statistical data of all experimental results in Table I for further comparison. The accuracy of using multiple monocular cameras is similar to that of using a single monocular camera. Nevertheless, as shown in Fig. 6, using multiple monocular cameras will observe more markers. It will improve the efficiency of HD map construction.

V. CONCLUSIONS & FUTURE WORK

This paper proposes a highly feasible framework for building a marking-level HD map using one or more monocular cameras, in which the homography matrix for IPM and the map are optimized at the same time. We evaluate the map accuracy in two test scenarios. The marking corner coordinates accuracy can be close to centimeter level, and the IPM matrix accuracy is similar to that of manually calibrated.

We highlight that it is a highly feasible and easy-to-extend solution to building HD maps at a low cost. In the future, we will extend the marking types to a wider range to generalize the method further.

REFERENCES

- [1] H. G. Seif and X. Hu, "Autonomous driving in the icity—hd maps as a key challenge of the automotive industry," *Engineering*, vol. 2, no. 2, pp. 159–162, 2016.
- [2] Y. Yu, P. Yun, B. Xue, J. Jiao, R. Fan, and M. Liu, "Accurate and robust visual localization system in large-scale appearance-changing environments," *IEEE/ASME Transactions on Mechatronics*, 2022.
- [3] M. Oliveira, V. Santos, and A. D. Sappa, "Multimodal inverse perspective mapping," *Information Fusion*, vol. 24, pp. 108–121, 2015.
- [4] B. Pan, J. Sun, H. Y. T. Leung, A. Andonian, and B. Zhou, "Cross-view semantic segmentation for sensing surroundings," *IEEE Robotics and Automation Letters*, vol. 5, no. 3, pp. 4867–4873, 2020.
- [5] H. A. Mallot, H. H. Bülthoff, J. Little, and S. Bohrer, "Inverse perspective mapping simplifies optical flow computation and obstacle detection," *Biological cybernetics*, vol. 64, no. 3, pp. 177–185, 1991.
- [6] W. Yang, Q. Li, W. Liu, Y. Yu, Y. Ma, S. He, and J. Pan, "Projecting your view attentively: Monocular road scene layout estimation via cross-view transformation," in *Proceedings of the IEEE/CVF Conference on Computer Vision and Pattern Recognition*, 2021, pp. 15536–15545.
- [7] C. Guo, K. Kidono, J. Meguro, Y. Kojima, M. Ogawa, and T. Naito, "A low-cost solution for automatic lane-level map generation using conventional in-car sensors," *IEEE Transactions on Intelligent Transportation Systems*, vol. 17, no. 8, pp. 2355–2366, 2016.
- [8] C. Lu, M. J. G. van de Molengraft, and G. Dubbelman, "Monocular semantic occupancy grid mapping with convolutional variational encoder-decoder networks," *IEEE Robotics and Automation Letters*, vol. 4, no. 2, pp. 445–452, 2019.
- [9] K. Mani, S. Daga, S. Garg, S. S. Narasimhan, M. Krishna, and K. M. Jatavallabhula, "Monolayout: Amodal scene layout from a single image," in *Proceedings of the IEEE/CVF Winter Conference on Applications of Computer Vision*, 2020, pp. 1689–1697.
- [10] T. Roddick and R. Cipolla, "Predicting semantic map representations from images using pyramid occupancy networks," in *Proceedings of the IEEE/CVF Conference on Computer Vision and Pattern Recognition*, 2020, pp. 11138–11147.
- [11] Y. B. Can, A. Liniger, O. Unal, D. Paudel, and L. Van Gool, "Understanding bird's-eye view of road semantics using an onboard camera," *IEEE Robotics and Automation Letters*, vol. 7, no. 2, pp. 3302–3309, 2022.
- [12] A. Saha, O. Mendez, C. Russell, and R. Bowden, "Translating images into maps," in *2022 International Conference on Robotics and Automation (ICRA)*, 2022, pp. 9200–9206.
- [13] J. Phillion and S. Fidler, "Lift, splat, shoot: Encoding images from arbitrary camera rigs by implicitly unprojecting to 3d," in *European Conference on Computer Vision*. Springer, 2020, pp. 194–210.
- [14] Q. Li, Y. Wang, Y. Wang, and H. Zhao, "Hdmapnet: An online hd map construction and evaluation framework," in *2022 International Conference on Robotics and Automation (ICRA)*. IEEE, 2022, pp. 4628–4634.
- [15] L. Deng, M. Yang, H. Li, T. Li, B. Hu, and C. Wang, "Restricted deformable convolution-based road scene semantic segmentation using surround view cameras," *IEEE Transactions on Intelligent Transportation Systems*, vol. 21, no. 10, pp. 4350–4362, 2019.
- [16] Y. B. Can, A. Liniger, D. P. Paudel, and L. Van Gool, "Topology preserving local road network estimation from single onboard camera image," in *Proceedings of the IEEE/CVF Conference on Computer Vision and Pattern Recognition*, 2022, pp. 17263–17272.
- [17] Z. Xu, Y. Sun, and M. Liu, "icurb: Imitation learning-based detection of road curbs using aerial images for autonomous driving," *IEEE Robotics and Automation Letters*, vol. 6, no. 2, pp. 1097–1104, 2021.
- [18] Z. Xu, Y. Sun, and M. Liu, "Topo-boundary: A benchmark dataset on topological road-boundary detection using aerial images for autonomous driving," *IEEE Robotics and Automation Letters*, vol. 6, no. 4, pp. 7248–7255, 2021.
- [19] Z. Xu, Y. Sun, L. Wang, and M. Liu, "Cp-loss: Connectivity-preserving loss for road curb detection in autonomous driving with aerial images," in *2021 IEEE/RSJ International Conference on Intelligent Robots and Systems (IROS)*, 2021, pp. 1117–1123.
- [20] Z. Xu, Y. Liu, L. Gan, X. Hu, Y. Sun, M. Liu, and L. Wang, "csboundary: City-scale road-boundary detection in aerial images for high-definition maps," *IEEE Robotics and Automation Letters*, vol. 7, no. 2, pp. 5063–5070, 2022.
- [21] J. Shu, S. Wang, X. Jia, W. Zhang, R. Xie, and H. Huang, "Efficient lane-level map building via vehicle-based crowdsourcing," *IEEE Transactions on Intelligent Transportation Systems*, 2020.
- [22] L. Mi, H. Zhao, C. Nash, X. Jin, J. Gao, C. Sun, C. Schmid, N. Shavit, Y. Chai, and D. Anguelov, "Hdmapgen: A hierarchical graph generative model of high definition maps," in *Proceedings of the IEEE/CVF Conference on Computer Vision and Pattern Recognition*, 2021, pp. 4227–4236.
- [23] W. Cheng, S. Yang, M. Zhou, Z. Liu, Y. Chen, and M. Li, "Road mapping and localization using sparse semantic visual features," *IEEE Robotics and Automation Letters*, vol. 6, no. 4, pp. 8118–8125, 2021.
- [24] M. Elhousni, Y. Lyu, Z. Zhang, and X. Huang, "Automatic building and labeling of hd maps with deep learning," in *Proceedings of the AAAI Conference on Artificial Intelligence*, vol. 34, no. 08, 2020, pp. 13255–13260.
- [25] Y. Zhou, Y. Takeda, M. Tomizuka, and W. Zhan, "Automatic construction of lane-level hd maps for urban scenes," in *2021 IEEE/RSJ International Conference on Intelligent Robots and Systems (IROS)*. IEEE, 2021, pp. 6649–6656.
- [26] A. Ranganathan, D. Ilstrup, and T. Wu, "Light-weight localization for vehicles using road markings," in *2013 IEEE/RSJ International Conference on Intelligent Robots and Systems*. IEEE, 2013, pp. 921–927.
- [27] W. Jang, J. An, S. Lee, M. Cho, M. Sun, and E. Kim, "Road lane semantic segmentation for high definition map," in *2018 IEEE Intelligent Vehicles Symposium (IV)*. IEEE, 2018, pp. 1001–1006.
- [28] W. Jang, J. Hyun, J. An, M. Cho, and E. Kim, "A lane-level road marking map using a monocular camera," *IEEE/CAA Journal of Automatica Sinica*, vol. 9, no. 1, pp. 187–204, 2021.
- [29] T. Qin, Y. Zheng, T. Chen, Y. Chen, and Q. Su, "A light-weight semantic map for visual localization towards autonomous driving," in *2021 IEEE International Conference on Robotics and Automation (ICRA)*, 2021, pp. 11248–11254.
- [30] T. D. Barfoot, *State Estimation for Robotics*. Cambridge: Cambridge University Press, 2017.
- [31] Y. Wu, A. Kirillov, F. Massa, W.-Y. Lo, and R. Girshick, "Detectron2," <https://github.com/facebookresearch/detectron2>, 2019.
- [32] Z. Qin, H. Wang, and X. Li, "Ultra fast structure-aware deep lane detection," in *The European Conference on Computer Vision (ECCV)*, 2020.
- [33] R. Hartley and A. Zisserman, *Multiple view geometry in computer vision*. Cambridge university press, 2003.